

PLASMA-SYNTHESISED ZINC OXIDE NANOPARTICLE BEHAVIOR IN LIQUIDS

¹David RUTHERFORD, ¹Jaroslav JÍRA, ²Kateřina KOLÁŘOVÁ, ³Iva MATOLÍNOVÁ,
²Zdenek REMEŠ, ¹Jaroslav KULIČEK, ⁴Dilli PADMANABAN, ⁴Paul MAGUIRE, ⁴Davide MARIOTTI,
¹Bohuslav REZEK

¹*Department of Physics, Czech Technical University, Prague, Czech Republic, EU, [*ruthedav@fel.cvut.cz](mailto:ruthedav@fel.cvut.cz)*

²*Institute of Physics, Czech Academy of Sciences, Prague, Czech Republic, EU*

³*Department of Surface and Plasma Science, Charles University, Prague, Czech Republic, EU*

⁴*School of Engineering, Ulster University, Belfast, N. Ireland*

<https://doi.org/10.37904/nanocon.2021.4318>

Abstract

Zinc oxide nanoparticles have been synthesized using non-thermal atmospheric pressure plasma (ZnO-NTP). We investigated the behavior of these ligand-free as a colloid suspension using different solvents, from deionized water to physiological saline and microbial culture broth. We found that the zeta potential of ZnO-NTP became more negative after exposure to microbial culture broth relative to water, which suggests increased colloid stability. Photoluminescence spectra of ZnO-NTP were similar regardless of liquid type, yet optical and fluorescent images of samples showed different agglomeration behavior depending on liquid type. Scanning electron microscopy images revealed large agglomerates of ZnO-NTP interacting with the surface of bacteria cells, ranging in size from 200 nm up to 2 μ m. We also studied effect of sub-lethal concentrations of ZnO-NTP on bacteria under illumination. There was no significant difference in viable bacteria concentration after 24h exposure to 10 μ g/mL ZnO-NTP relative to untreated control irrespective of sample illumination.

Keywords: Zinc oxide, nanotechnology, colloid suspension, bacteria

1. INTRODUCTION

Non-thermal plasma (NTP) have emerged as a promising technology for the synthesis of highly crystalline nanoparticles [1,2]. Commercially available nanoparticles produced on an industrial scale can result in the introduction of unwanted impurities that can negatively impact their integration into downstream applications. For example, according to the material safety data sheet for spherical zinc oxide nanoparticles (ZnO NP), there may be traces of aluminum oxide present [3]. NTP can be described as a green synthesis technique, in that no toxic chemicals are required in the generation of ZnO NP. There are a number of examples where NTP have been used to synthesize ZnO NP [4–7]. However, their interaction with complex liquids of biological relevance remains yet to be fully explored.

Nanoparticles are greatly influenced by their surrounding environment due to the high surface area to volume ratio making them highly responsive to the water chemistry of the solvent when in a colloidal suspension. Thus, their behavior in the colloid as well as inherent properties can be suppressed or enhanced by surface interaction with other molecules that are also present in the liquid such as proteins or carbohydrates. Our prior computer simulations showed that the interaction between amino acids and zinc oxide surface involved covalent bonding and not merely due to passive adsorption [8].

Here, we synthesize ZnO nanoparticles by using non-thermal atmospheric-pressure plasma (ZnO-NTP) and characterize its material properties under specific conditions. The nanoparticles are then introduced in liquids

of varying ionic and biomolecule content and we measure the resulting optical and colloidal and microbiological effects.

2. MATERIALS AND METHODS

2.1. Nanoparticle synthesis

ZnO nanoparticles were synthesized using a non-thermal plasma reactor (**Figure 1 A**) consisting of a hollow stainless steel housing with a quartz tube (1 mm outer diameter, 0.7 mm inner diameter) and a pure zinc wire (0.5 mm, 99.99%, Alfa Aesar) positioned inside the housing attached to ground. The wire along with the quartz tube was placed inside a copper plate which was connected to a radio-frequency (40W, 13.56 MHz) power source connected using a matching network. A mass flow controller delivered helium (He, 0.3 slm) into the housing and a gas-phase microplasma ignited within the quartz tube and interacted with the zinc wire. Generated nanoparticles (ZnO-NTP) were transported away from the microplasma by the gas flow and collected downstream on a clean Si (intrinsic) substrate at a rate of 0.3 mg/s. The dry powder was then transferred to a clean vial and used for characterization analyses.

2.2. Nanoparticle characterization

The crystallographic profile of the synthesized ZnO-NTP was explored by high-resolution transmission electron microscope (TEM, Jeol JEM02100 F) coupled to selected area electron diffraction (SAED) to determine particle morphology, phase and size distribution after the synthesis. The transmission microscopy images and SAED patterns were analyzed using ImageJ (1.48v) software for particle size distribution and d-spacing calculation. ZnO-NTP optical properties were probed using UV-visible spectroscopy (UV-vis, PerkinElmer LAMDA 365), and photoluminescence (PL, WITec, alpha300 RAS) after exposure to liquids: demineralized water (dH₂O, Resta), 0.9% sodium chloride (NaCl, Penta) and Mueller Hinton broth (MHB, Oxoid). The size distribution and zeta potential of ZnO-NTP after exposure to different liquids was analyzed by dynamic light scattering (ZetaSizer, Malvern).

A stock solution of ZnO-NTP and dilutions thereof were made using demineralized H₂O (<1 μS/cm) and subjected to sonication prior to analysis (160 W for 30 min, DT31, Sonorex Digitec). For PL and zeta potential measurements, ZnO-NTP were first removed from dH₂O by centrifugation (30min at 13k rpm, MPW-150R) followed by resuspending in the same volume of a different liquid type. ZnO-NTP were subsequently vortexed in either dH₂O, 0.9 % NaCl or MHB (8000 rpm, 1 min) before sonication under the same conditions previously used. The liquid was removed by centrifugation again and ZnO-NTP were re-suspended in dH₂O for a final round of sonication before analysis.

2.3. Nanoparticle interaction with bacteria

Escherichia coli (*E. coli*, CCM 3954, Brno) were resuscitated on Mueller Hinton agar (MHA, Carl Roth) plates and cultivated overnight (37 °C). The following day, 1 colony was removed and resuspended in 100 mL MHB and placed on an orbital shaker located inside an incubator (150 rpm for 24 h at 37 °C). Next, the bacteria were adjusted to McFarland's Density 1.0 in fresh MHB using a densitometer (Biosan), then subsequently diluted 1:1000 in fresh MHB to an approximate concentration of 1×10⁵ cfu/mL. 1 mL of ZnO-NTP in dH₂O (100 μg/mL) was added to 9 mL *E. coli* in a 50 mL Falcon tube and placed inside reverse spin bioreactors (2000 rpm/1s, RTS-1, BioSan) with and without illumination (Reflekt). The white light source was selected based on overlapping spectral output and UV-vis absorbance profile of ZnO-NTP (i.e. between 400-500 nm). The concentration of viable bacteria was measured at the start and again after 24 hours by performing a 1:10 dilution series using 0.9% NaCl and inoculating onto MHA before incubating (37° C for 24 h). 100 μL of the bacteria-ZnO-NTP mixture was removed after 24 h and diluted 1:100 in dH₂O then 10 μL was drop-casted

onto silicon wafer for SEM analysis (MIRA III, Tescan). It was not possible to image ZnO-NTP in 0.9% NaCl or MHB using SEM due considerable crystallization of salts and other components on the substrate.

3. RESULTS

3.1. Morphology, UV-vis and phase

Morphology of the synthesized ZnO-NTP collected in ethanol was probed using TEM and the images showed uniform grain-like shaped particles (**Figure 1 (B)**). One can see that the particles are well dispersed with individual primary particles clearly visible. Analysis of TEM images revealed the mean particle size was 18.6 ± 6.5 nm and there was a log normal distribution with regards to particle diameter and number (**Figure 1 (C)**). **Figure 1 (D)** shows a Tauc plot derived from UV-vis absorbance data of ZnO-NTP in ethanol and the energy band gap (E_g) calculated to be approximately 3.22 eV. **Figure 1 (E)** shows the SAED profile of ZnO-NTP that displays a hexagonal wurzite phase (space group $P_{63}mc$, indexed based on JCPDF file # 65-3411).

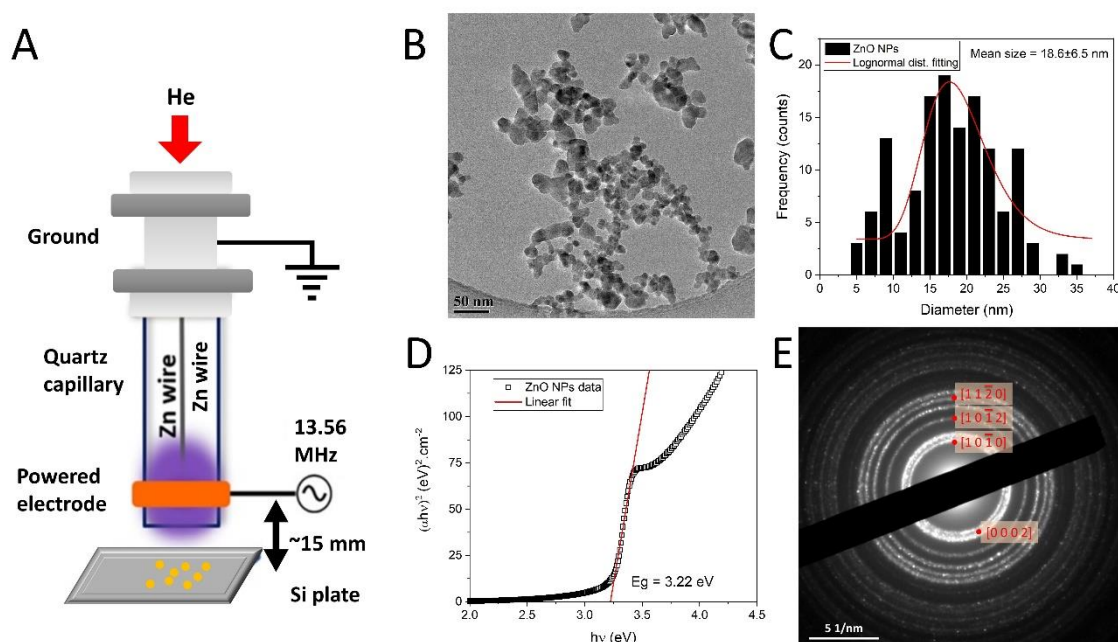


Figure 1 (A) Schematic diagram of the non-thermal atmospheric pressure plasma system with zinc wire used for ZnO nanoparticle synthesis (ZnO-NTP). (B) TEM image of ZnO-NTP. (C) Histogram showing size distribution analysis from TEM images. (D) Tauc plot derived from ZnO-NTP absorbance data obtained using UV-vis spectroscopy (E) SAED profile of ZnO-NTP.

3.2. Zeta potential and DLS

ZnO-NTP were first exposed to dH_2O and then suspended in 3 liquid types during sonication before being resuspended in dH_2O for size distribution and zeta potential analysis. From **Figure 2**, one can see three main size fractions from in MHB-exposed ZnO-NTP, specifically at 79 nm, 712 nm, and 5560 nm. This correlates well with the zeta potential measurements, where there were also three peaks detected, at -36.6 mV, -23.4 mV and -7 mV. There were also three distinct size fractions observed from dH_2O -exposed ZnO-NTP, at 396 nm, 1484 nm and 4801 nm. However, the different sized particles generated a single peak for zeta potential measurement at -12.4 ± 0.4 mV. ZnO-NTP exposed to 0.9% NaCl became more positive with an observed value of 5.3 ± 0.6 mV, however DLS analysis was unable to detect particles below 10 μm even after extensive sonication prior to measurement which makes the value unreliable.

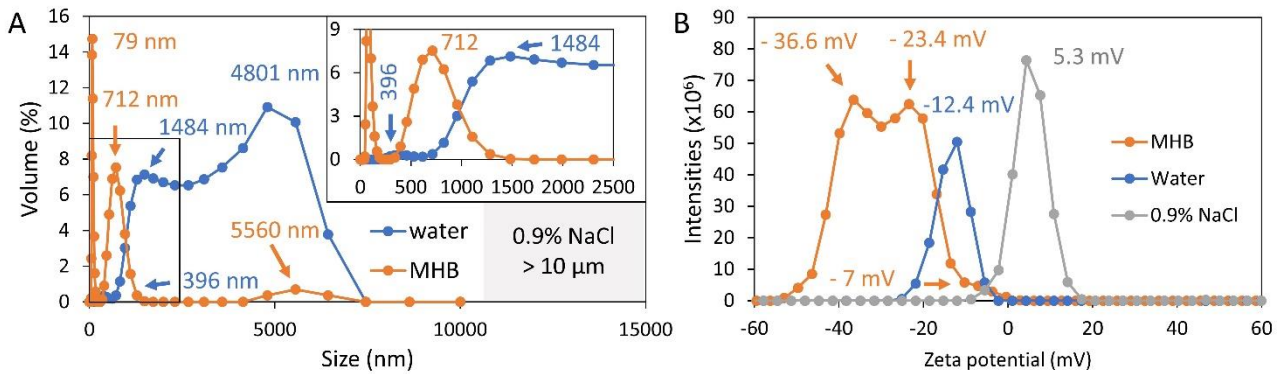


Figure 2 ZnO-NTP size distribution according to volume (A) and intensities with corresponding zeta potential (B). Numbers inset indicate measured values and arrows point to the specific data

3.3. Photoluminescence (PL)

Room temperature PL spectra from ZnO-NTP dried under ambient conditions on Si wafer and illuminated using blue laser (430-435 nm) and filter can be seen in **Figure 3 (A)**. The line profile of each PL spectra is similar regardless of liquid type, with a dominant peak between 600-610 nm and two troughs located either side at 590 nm and 615 nm. No new peaks were detected from any ZnO-NTP and the maximum PL intensity was recorded at the same wavelength in each sample (606 nm).

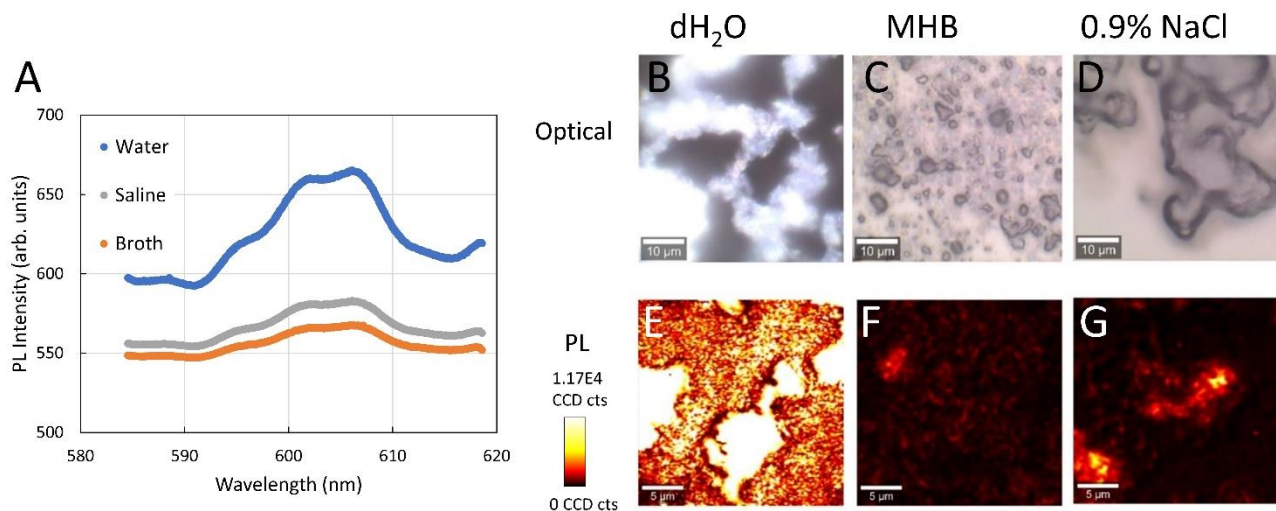


Figure 3 PL spectra of ZnO-NTP illuminated by blue light (430-435 nm) using 570 nm filter (A). Optical (B-D) and fluorescent (E-G) images of ZnO-NTP that generated the spectra in A

Optical image of ZnO-NTP exposed to dH₂O showed large agglomerates (**Figure 3 (B)**) with strong fluorescent emission (**Figure 3 (E)**). ZnO-NTP exposed to 0.9 % NaCl also showed agglomeration (**Figure 3 (D)**), but without the strong fluorescent emission seen previously for dH₂O-exposed ZnO-NTP (**Figure 3 (G)**). The optical image of MHB-exposed ZnO-NTP showed the most dispersed arrangement of particles (**Figure 3 (C)**) with the least amount of fluorescence (**Figure 3 (F)**).

3.4. Interaction with bacteria (cfu/mL & SEM)

Reverse spin bioreactors enabled interaction between a low concentration of ZnO-NTP (10 μg/mL) and *E. coli* in MHB. From our previous work, 10 μg/mL ZnO did not inhibit growth of *E. coli* in MHB. Here, we employed yet another different type of ZnO nanoparticles (in shape and size) and studied also the effect of illumination

with a non-bactericidal white light source having spectral output overlapping with UV-vis absorbance profile of ZnO-NTP (i.e. between 400-500 nm).

There was no significant difference in *E. coli* concentration after 24 h exposure to ZnO-NTP relative to unexposed (control) regardless of illumination ($P > 0.05$, **Figure 4 (A)**). SEM image of *E. coli*-ZnO-NTP taken after 24 h exposure revealed small particles resting on the cell surface, as well porous superstructures that were large enough to interact with whole bacteria cells (**Figure 4 (B)**).

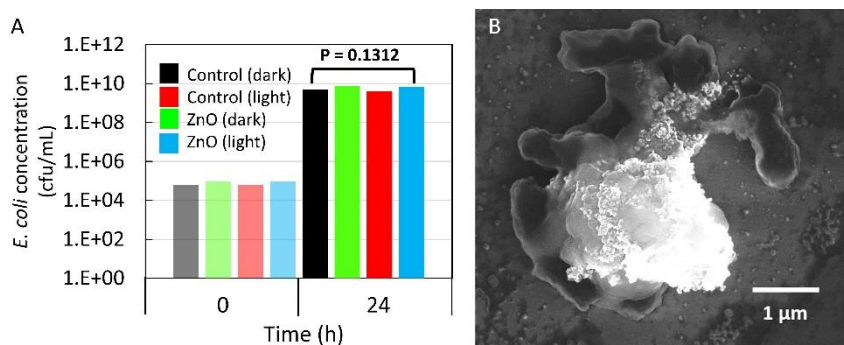


Figure 4 (A) Bar chart displaying the concentration of viable *E. coli* at the start of the experiment (0) and after 24 h exposure to 10 $\mu\text{g/mL}$ ZnO-NTP in reverse spin bioreactors. (B) Scanning electron microscopy image showing a size range of ZnO-NTP aggregates interacting with multiple *E. coli* cells.

4. DISCUSSION

Novel non-thermal plasma technique has been demonstrated to synthesize ZnO nanoparticles of specifically small size, shape and quality at room temperature without any harsh chemicals or large vacuum systems. The non-equilibrium nature inside the discharge region causes reactions occur rapidly and continue in the afterglow where atmospheric gases and humidity gain influence that can lead to the formation of reactive oxygen and nitrogen species (RONS). Nanoparticle formation arises from plasma interaction with nanoparticle precursor atom/molecule in either the feed gas mixture, liquid solution, or solid substrate. Here, a solid zinc wire was placed inside an rf-driven non-thermal plasma using He as the feed gas which carried ZnO-NTP away from the core plasma region for collection. TEM image of ZnO-NTP showed uniform grain morphology with a log normal size distribution and mean particle diameter of 19 nm, however there were also many particles at around 10 nm and 30 nm. The same plasma system was also capable of synthesizing smaller ZnO quantum dots with a mean particle diameter of 1.9 nm when operating under the same power conditions but using argon instead of helium [7]. This suggests that it is possible to control the size of the nanoparticle synthesized using non-thermal plasma by varying the feed gas composition.

ZnO-NTP showed typical UV light absorbance behavior, with a sharp peak at the maximum absorbance wavelength of 370 nm and the calculated energy band gap from Tauc plot derived from absorbance data was 3.22 eV, which is in good agreement with the literature [9]. ZnO-NTP also exhibited photoluminescence when illuminated with light of smaller energy than the band gap ($\lambda = 430\text{-}435$ nm). The PL spectra are similar, and the maximum PL intensity remained at 606 nm in all samples irrespective of liquid type. Thus, the PL spectra are robust in biological environment. Such PL emission arises due to ZnO surface defects [9,10].

The observed differences in PL intensities between ZnO-NTP exposed to different liquid types are most likely due to variation in sample thickness which is influenced in part by material agglomeration as shown in the optical images in **Figure 3**. The PL microscopic images showed high particle agglomeration in water, which could account for the higher PL signal compared to 0.9% NaCl and MHB. Nevertheless, prior reports showed that the PL emission can be quenched by amino acid residues from proteins bound to the surface of ZnO [11]. Quenching of the fluorescence of BSA due to interaction with ZnO NP through the formation of stable ground

state complexes was also observed [12], highlighting the fact that both ZnO NP and BSA can influence each other's properties and it is not solely the action of one or the other. Such complex interaction could be occurring in our case, where biomolecules contained in MHB may coat ZnO-NTP, forming a protein/carbohydrate corona that results in PL emission quenching.

Protein coronas also tend to increase particle aggregation due to enhanced particle-particle interaction thereby creating a less well dispersed population. Yet the PL images showed that MHB-exposed ZnO-NTP to be the most dispersed material compared to dH₂O and 0.9% NaCl-exposed ZnO-NTP.

Zeta potential analysis of MHB-exposed ZnO-NTP also implied a more dispersed population compared to dH₂O and 0.9% NaCl-exposed ZnO-NTP. There were three distinct peaks in both zeta potential measurement and size distribution for MHB-exposed ZnO-NTP, two pronounced peaks and one much smaller. The values of the two pronounced peaks (-36.6 mV and -23.4 mV) were more negative than the single peak from dH₂O-exposed ZnO-NTP of -12.4 mV. A higher absolute value of zeta potential can result in a more disperse population of particles in the suspension due to better electrostatic repulsion of nanoparticles. Zeta potential of ZnO also became more negative after exposure to biomolecules such as BSA [13], in agreement with our data in MHB. The third peak from zeta potential measurement was less negative than the prior two (-7 mV) which may have been generated from the larger size fraction at 5560 nm which accounted for a small percentage of the total volume of particles. For MHB-exposed ZnO-NTP, one can assume that the three separate peaks observed in zeta potential analysis were generated from the three different size fractions. However, this was not the case for dH₂O-exposed ZnO-NTP where there were three size fractions observed yet only one zeta potential peak. This suggests that the effect of MHB on the size and zeta potential of ZnO-NTP is more pronounced than for dH₂O. The two smaller size fractions from MHB-exposed ZnO-NTP (79 nm and 712 nm) were smaller than the two smallest size fractions from dH₂O-exposed ZnO-NTP (396 nm and 1484 nm) which also suggests a more dispersed population of particles with smaller aggregates. However, even the smallest size fraction observed (79 nm) was larger than the primary particle size seen from TEM image in **Figure 1** (19 nm), therefore some aggregation of primary particles occurs on MHB-exposed ZnO-NTP. Upon exposure to 0.9% NaCl, the zeta potential of ZnO-NTP shifted to a less negative value of 5.3 mV. This trend was also observed for ZnO NP exposed to increasing NaCl concentrations, from -28 mV to -2 mV, however the highest concentration of NaCl used in that study and produced the least negative zeta potential was x30 less than what was used in our experiments [14].

It has been reported in the literature that the smaller the nanoparticle, the greater the antibacterial effect [15]. This is also true for aggregates of particles and one might expect greater antibacterial effect from more dispersed colloidal suspension. However, we have previously shown that particle morphology is also important in the antibacterial effect of ZnO in MHB, and particles with uniform rounded morphology were less antibacterial than particles composed of many needle-like clusters [16]. At the same concentration used here (10 µg/mL), there was no significant difference in viable bacteria relative to unexposed bacteria regardless of ZnO size or shape. At higher concentrations (≥100 µg/mL), the needles were still sufficiently sharp even after being coated with components of MHB to inactivate bacteria by puncturing the cell membrane, whereas the more rounded particles tended to aggregate on the cell surface. A non-bactericidal white light source with overlapping spectral output and UV-vis absorbance profile of ZnO-NTP was chosen to try and enhance the antibacterial effect (i.e. between 400-500 nm). Visible light photoinactivation of bacteria mediated by ZnO has been reported that was mainly attributed to the bactericidal effect of zinc ions [17]. We have previously shown that without illumination the concentration of zinc ion produced in MHB would not be great enough to become cytotoxic due to the components in MHB scavenging zinc ion before interacting with bacteria [16]. However, hydrogen peroxide was measured from illuminating a much higher concentration of commercially available ZnO (2 mg/mL) using the same experimental set up and illumination source used here (unpublished data).

5. CONCLUSION

Variation in the physicochemical properties of ZnO-NTP nanoparticles due to the effect of exposure to various liquids was observed. Interestingly, the best dispersion was observed in cell culture MHB medium, providing smallest aggregates (79 nm) and most negative zeta potential (-36.6 mV). The PL spectra remained unaffected. In the employed sub-lethal concentration the ZnO-NTP nanoparticles rather enhanced the bacterial growth, as observed for other ZnO NP types before. Yet illumination did not lead to any bactericidal effect, unlike for other ZnO nanoparticle types. This must be related with specific nanoparticle preparation using non-thermal plasma. This means that photoexcitation and PL spectra can be used as a robust sensing pathway in biological environment.

ACKNOWLEDGEMENTS

The presented work was supported financially by the project GACR 19-02858J.

REFERENCES

- [1] KORTSHAGEN, U. R., SANKARAN, R. M., PEREIRA, R. N., GIRSHICK, S. L., WU, J. J. and AYDIL, E. S. Nonthermal Plasma Synthesis of Nanocrystals: Fundamental Principles, Materials, and Applications *Chem. Rev.* 2016, vol. 116, pp. 11061–127.
- [2] CHIANG, W-H, MARIOTTI, D., SANKARAN, R. M., EDEN, J. G. and OSTRIKOV, K. (Ken) Microplasmas for Advanced Materials and Devices *Advanced Materials* 2020, vol. 32, 1905508.
- [3] Anon 2019 Material Safety Data Sheet (MSDS) - ZnO
- [4] FELBIER, P., YANG, J., THEIS, J., LIPTAK, R. W., WAGNER, A., LORKE, A., BACHER, G. and KORTSHAGEN, U. Highly Luminescent ZnO Quantum Dots Made in a Nonthermal Plasma *Advanced Functional Materials*. 2014, vol. 24, pp. 1988–93
- [5] TSUMAKI, M., SHIMIZU, Y. and ITO, T. Size-controlled sub-micrometer spheroidized ZnO particles synthesis via plasma-induced processing in microdroplets *Materials Letters*. 2016, vol. 166, pp. 81–4.
- [6] JAIN, G., MACIAS-MONTERO, M., VELUSAMY, T., MAGUIRE, P. and MARIOTTI, D. Porous zinc oxide nanocrystalline film deposition by atmospheric pressure plasma: Fabrication and energy band estimation. *Plasma Process Polym.* 2017, vol. 14, 1700052.
- [7] JAIN, G., ROCKS, C., MAGUIRE, P. and MARIOTTI, D. One-step synthesis of strongly confined, defect-free and hydroxy-terminated ZnO quantum dots *Nanotechnology* 2020, vol. 31, 215707.
- [8] REZEK, B., HEMATIAN, H., JÍRA, J., RUTHERFORD, D., KULIČEK, J., UKRAINTSEV, E. and REMEŠ, Z. Microscopic Study of Bovine Serum Albumin Adsorption on Zinc Oxide (0001) Surface *physica status solidi (a)* 2021, vol. 218, 2000558.
- [9] ISLAM, S. and AKYILDIZ, H. I. Immobilization of ZnO thin films onto fibrous glass substrates via atomic layer deposition and investigation of photocatalytic activity *J Mater Sci: Mater Electron*. 2021, vol. 32, pp. 27027–43.
- [10] DJURIŠIĆ, A. B., LEUNG, Y. H., TAM, K. H., HSU, Y. F., DING, L., GE, W. K., ZHONG, Y. C., WONG, K. S., CHAN, W. K., TAM, H. L., CHEAH, K. W., KWOK, W. M. and PHILLIPS, D. L. Defect emissions in ZnO nanostructures. *Nanotechnology*. 2007, vol. 18, 095702.
- [11] BHUNIA, A. K., KAMILYA, T. and SAHA, S. Temperature Dependent and Kinetic Study of the Adsorption of Bovine Serum Albumin to ZnO Nanoparticle Surfaces *ChemistrySelect*. 2016, vol. 1, pp. 2872–82.
- [12] HANSDA, C., MAITI, P., SINGHA, T., PAL, M., HUSSAIN, S. A., PAUL, S. and PAUL, P. K. Photophysical study of the interaction between ZnO nanoparticles and globular protein bovine serum albumin in solution and in a layer-by-layer self-assembled film *Journal of Physics and Chemistry of Solids* 2018, vol. 121, pp. 110–20.
- [13] BHUNIA, A. K., KAMILYA, T. and SAHA, S. Synthesis, Characterization of ZnO Nanorods and its Interaction with Albumin Protein *Materials Today: Proceedings*. 2016, vol. 3, pp. 592–7.
- [14] PENG, Y.-H., TSO, C., TSAI, Y., ZHUANG, C. and SHIH, Y. The effect of electrolytes on the aggregation kinetics of three different ZnO nanoparticles in water *Science of The Total Environment*. 2015, vol. 530–531, pp. 183–90.

- [15] KAUSHIK, M., NIRANJAN, R., THANGAM, R., MADHAN, B., PANDIYARASAN, V., RAMACHANDRAN, C., OH, D-H. and VENKATASUBBU, G. D. Investigations on the antimicrobial activity and wound healing potential of ZnO nanoparticles *Applied Surface Science* 2019, vol. 479, pp. 1169–77.
- [16] RUTHERFORD, D., JÍRA, J., KOLÁŘOVÁ, K., MATOLÍNOVÁ, I., MIČOVÁ, J., REMEŠ, Z. and REZEK, B. Growth Inhibition of Gram-Positive and Gram-Negative Bacteria by Zinc Oxide Hedgehog Particles. *IJN*. 2021, vol. 16, pp. 3541–54.
- [17] SAPKOTA, A., ANCENO, A. J., BARUAH, S., SHIPIN, O. V. and DUTTA, J. Zinc oxide nanorod mediated visible light photoinactivation of model microbes in water *Nanotechnology* 2011, vol. 22, 215703.